ADAPTIVE SAMPLING PLAN DESIGN METODOLOGY FOR REVERSE ENGINEERING ACQUISITION

ADAPTIVE SAMPLING PLAN DESIGN METODOLOGY FOR REVERSE ENGINEERING ACQUISITION

E. Vezzetti

Dipartimento di Sistemi di Produzione Ed Economia dell'Azienda, Politecnico di Torino, Corso Duca degli Abruzzi 24, 10129,Torino, Italy

Tel.: +39 011 5647294; Fax: +39 011 5647299; e-mail: enrico.vezzetti@polito.it

Abstract

Reverse Engineering is a technology that generates a virtual representation of an existing part based on point data acquisition with measuring techniques. Different technologies could be employed to obtain a virtual representation of a physical model, but the use of a solution (3D scanner) rather than another, could provide significant different results because the available 3D scanners are characterised by different performances (resolution, accuracy, …)

But even if great attention should be oriented to the selection of the most appropriate 3D scanner device, this is not enough for assuring to obtain a consistent virtual representation of the physical model. The selection of the right 3D scanner could guarantee an improvement in the points acquisition precision, but it could not assure an efficient points distribution in term of number and locations. These two parameters make part of the acquisition strategy that would be implemented once the 3D scanner has been identified.

In order to support next steps of the reverse engineering cycle (segmentation, fitting, …), the acquisition phase should provide an organised points cloud obtained as the result of a consistent sampling plan.

For this reason this paper wants to propose a methodology to define a selectively sampling plan, with grid dimensions related with the complexity of the local surface region analysed.

Keywords: Reverse Engineering, Sampling Strategy, 3DScanner Performances, Free-Form

1.0 Introduction

3D Scanner usually acquires the object surface using a constant grid which dimensions depend on the technology employed [1-7]. Unfortunately the different complexity levels that often could cover an object surface (Free-Form) originate two possible situations: some surface regions, characterised by simple profiles, could be described by redundant information, while some others, characterised by significant more complex profiles, could present insufficient data. Both the situations are critical for the reverse engineering approach, in particular for surface fitting, because in the first scenario, it will spend a lot of time in order to fit simple surfaces with many redundant points, while in the other it could create non conformal surfaces for the absence of intermediate information in some areas.

Sometimes these problems are solved during the pre-processing and segmentation phases by the use of filters [8], when the points number is too high and the morphological information are redundant, and by the use of thickening strategies [9] when the point cloud is too scattered. But both the solutions could introduce non consistent information because these software operations make statistical hypothesis on the possible surface behaviour without any possible validation with the real object.

In order to reduce the error percentage during the reconstruction phase it is necessary to move the in-fitting and de-fitting operations already in the acquisition phase designing an adaptive sampling plan for the digitalisation of the real object surface instead of the constant grid approach.

One of the most common approaches in the identification of and adaptive sampling plan depend on the experience of the 3D scanner operator. He in fact, before starting the acquisition phase, studies the surface complexity, dividing the object in different regions in relation with their complexity, deciding then the optimal pitch for every region identified. But all these operations are developed simply with the use of a visual analysis that drives an iterative pitch hypothesis definition process, that ends when the operator is satisfied by the points cloud obtained. This approach feels the absence of a univocal and objective decisional parameter to define the real best acquisition pitch, causing the necessity to develop many different tests before finding the best solution.

For this reason it is necessary to find a structured and reliable methodology that could help the 3D scanner operator to identify automatically a specific pitch related to the local acquired region and its local complexity.

Most of the works already developed on the study of a selective acquisition pitch [10 - 12] have been developed not for reverse engineering application but more in the specific for computer inspection operations, often working with the availability of the CAD model. Interesting solutions have been presented by Cho and Kim [13] and by Li, Barhak, Guskov and Blake [14], always developed for inspection purposes, which proposed strategies for selecting the distribution of discrete data points on sculptured surfaces. The first strategy consists of two stages of surface subdivision. The first stage uniformly divides the surface into a number of regions. The second stage uniformly subdivides each region into smaller sub-regions, then it calculates the surface mean curvature at a uniform grid of points displaced on the sub-region, and ranks the sub-regions according to their average curvature values.

While the previous method proposed inspection strategies working on differentiable geometries this paper, starting only from a first raw points cloud, without the availability of any other mathematical models, wants to propose a methodology for designing a selective sampling plan for providing to surface fitting strategies the best organised points cloud.

2.0 Selective sampling strategy: methodology

The proposed method aims to identify a selective sampling plan, adaptive pitch, which changes locally in relation with the surface complexity of the region analysed (Fig.1).

In order to reach this target, first of all it has been necessary to implement a segmentation strategy able to divide the entire object surface in different complexity regions, working firstly on a first raw point cloud. The Gaussian curvature K (Fig.2) has been already employed [15] as morphological descriptor with the following formulation:

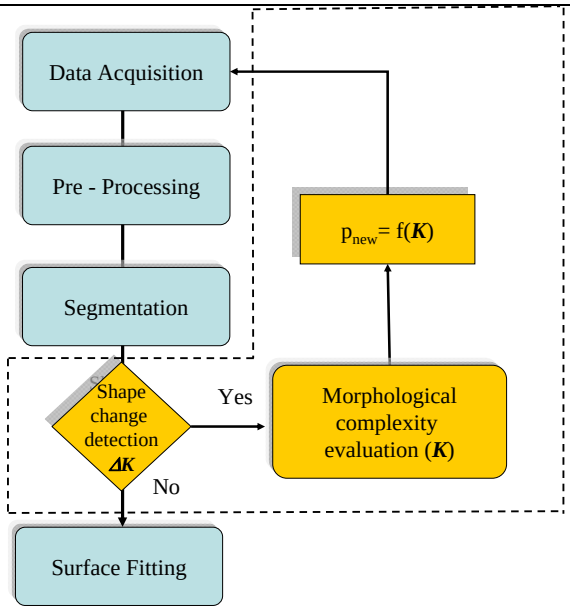

Figure 1: Proposed methodology flow chart

$$K = 2\pi - \sum_i \vartheta_i \,, \qquad (1)$$

where ϑ_i indicates each angle sharing the same central node of a discrete neighbourhood.

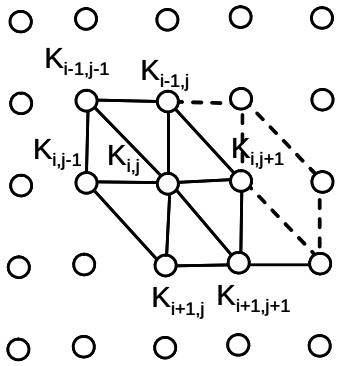

Figure 2: Morphological complexity evaluation: For every reference region the algorithm compares the central node curvature $K_{i,j}$ with the other boundary nodes curvature

Working with a statistical threshold *U(K)*, correlated with the measurement uncertainty of the 3D scanner, and with the variation of the curvature *K*, *ΔK*, it has been possible to identify those regions showing significant shape changing and so needing a deeper acquisition.

$$U(K) = t \cdot \sqrt{\{\mathbf{C}\}^T_{1X21}\left[\mathbf{s}^2(\xi)\right]_{21X21}\{\mathbf{C}\}_{21X1}} \,, \qquad (2)$$

$$\left|K_{i,j} - K_{l,m}\right| \geq U\left(K_{i,j}\right) \text{ where } l = (i-1),(i+1); \quad m = (j-1),(j+1). \tag{3}$$

$U(K)$: Extended uncertainty

$\{C\}$: represents the vector collecting the sensibility coefficients $\left(\frac{\partial K}{\partial \xi_i}\right)$, where $\xi = x \wedge y \wedge z$

Once segmented the points cloud the proposed approach selects the optimal pitch of next acquisitions for every regions identified by using the morphological descriptor *K* (1).

2.1 Selective sampling plan design: points cloud splitting

Talking about Free-Form surfaces it is possible to find different mathematical formalisations. Moving from Bezier (Fig.3), till arriving to B-Splines, it is possible to obtain very smooth geometries with very different complexities, managed with a variety of mathematical parameters. But all these methods are known to work well when talking about ideal surfaces generated with the help of computer aided design tools (CAD), which let the creation of a wide range of possible ideal shapes, by designing and managing only some control points or boundary curves [16].

The situation is completely different when talking about reverse engineering and 3D scanner, where Free-Form surfaces could be seen in a simpler format given by punctual three-dimensional coordinates acquired on the physical object surface. This situation is due to reverse engineering methodology often working on physical objects without a defined or accessible mathematical model by using 3D scanner devices (Fig.4).

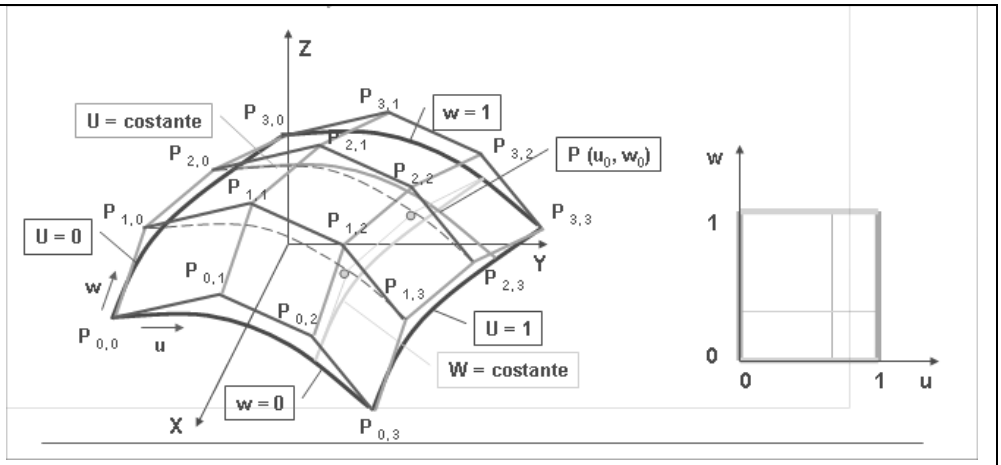

Figure 3: Example of ideal Free-Form surface developed with the use of Bezier Formula

Considering that the points cloud is usually the only available information about the shape of the acquired object, it is necessary to extract from it all the possible morphological data.

For what concerns Free-Form surface, they have been codified [16] basing only on purely geometrical assumptions, even if such anomalies as scrapes, digs, corners, bents or bumps have been present, they would have been considered as “non-Free-Form features” because they could have not ever locally been seen as connected compositions of simpler geometries, such as spheres, cones, cylinders (“ideal definition”). All the

approaches based on this previous criterion, focusing on the ideal characteristics of such surfaces, then recommended pitch improving in those areas affected by non-Free-Form anomalies.

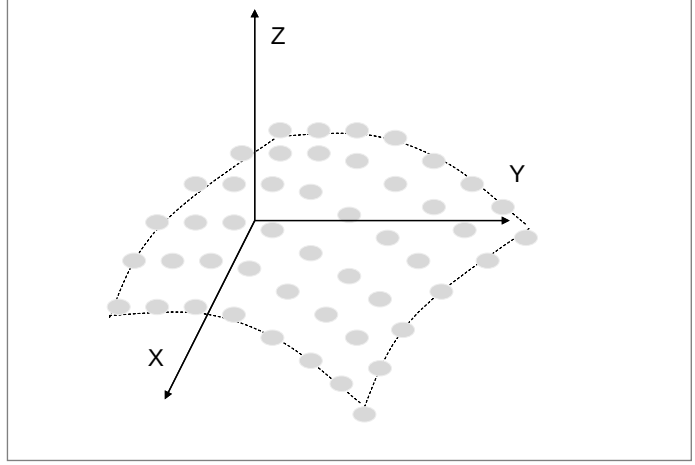

Figure 4: Example of Free-Form surface described as points cloud

In order to design a new more general purpose approach, thus involving a wider range of surfaces to perform further analyses, in this paper a new point of view is presented, considering the most common Free-Form surfaces sampling format, i.e. the points cloud as the very output of metrological devices, such as 3DScanners and CMMs.

In the former case, the points position within the cloud will depend on metrological information (related to scanning device accuracy, resolution etc) on purely geometrical data (original design, virtual curvature design) and those shape anomalies due to manufacturing systems (tolerances, roughness etc.).

On the other hand, the latter cloud would be an ideal one, for example obtained by extracting a grid of point from a CAD model, so only purely geometrical information, coming from the original CAD model, could influence the points position.

From this point of view, while observing a Free-Form surface, it is quite simple to subjectively distinguish those morphological features not reflecting the “ideal definition” [16] from those complying with it.

For example, shape features like scrapes, digs, corners, bents and bumps could be due either to the manufacturing system or the 3D Scanner uncertainty. On the other hand, the Free-Form surface could have already been designed with the presence of bents and bumps, if it were planned so in the specific original project.

Basing on such considerations the proposed approach wants to increase the number of sampling points where the surface morphology is complex, while reducing the scanning plan set where the data are redundant employing a 3D scanner Free-Form codification that distinguishes the sampled surface in two elements: those features which can be reasonably considered to follow the “ideal Free-Form definition”[16] and those which could be called “anomalies” (Fig. 5), independently from their causes and origins (the manufacturing system uncertainty or the scanning device precision).

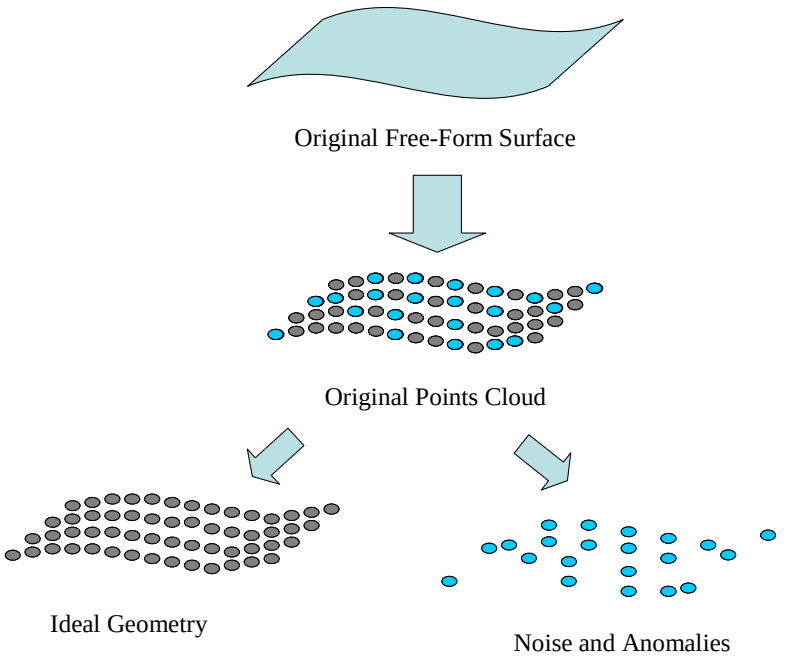

Figure 5: Free - Form surface decomposition: ideal geometry component and noise and anomalies component

As in this new approach the information conveyed by point cloud is to be split in two components, also the adopted decisional parameter to define local complexity will have to show the same property. Referring to a previous work [15] the most reliable morphological descriptor has been shown to be the Gauss Curvature *K*, measured as nodal angular excess (1).

As a consequence, the curvature *K* formulation has to be shifted in two components. As introduced before, the former component should be related to the nominal shape of the acquired Free-Form surface, while the latter includes the 3D device metrological uncertainty and all the possible geometrical anomalies due to the manufacturing process the original physical object has been created by.

Each component has been studied trough the use of some benchmarking surfaces, which has been virtually generated as point clouds, thanks to numerical simulation tools. Working with a points cloud preliminary triangulation, based on a first raw acquisition [15], each surface has been characterized by two main morphological components: the ideal geometry and a known statistical distributed noise. This expedient has been adopted to easily study the two components roles, that have been supposed to describe the curvature *K* .

2.1.1 Curvature *K* Ideal geometry component formulation

The former component will be first analysed. For what concerns wiggly differentiable geometries, showing opportune characteristics of curvature distribution, this parameter is known to be directly related to the osculating sphere radius [17]. For this reason, the design of the first benchmarking geometry used to experimentally study this curvature component has been oriented to a family of spherical surfaces which have been obtained only by radius varying, without any noise component. The radius values have been chosen among the most recurrent ones while dealing with Free-Form surfaces approximation (face-shapes, sheet-forms etc.). The following scanning pitches *p* have been selected around the largest grid dimension, thus allowing the most

significant values of nodal curvature to be obtained.

Moving from differentiable varieties to discrete ones, and especially referring to triangulations, the influence of the acquisition pitch will have to be encountered. As could be seen in the results (Tab. 1), it is possible to identify an analytical relation between the curvature *K*, sphere radius and acquisition pitch.

ρ [mm]	*K* [rad]; *p*=10mm	*K* [rad]; *p*=5mm	*K* [rad]; *p*=3,3mm
40	0,080	0,020	0,008
35	0,120	0,025	0,011
30	0,150	0,035	0,014
25	0,225	0,047	0,020
20	0,400	0,072	0,030

Table 1: Curvature *K* values for a family of spheres obtained by radius variation, with three different acquisition pitches.

The obtained formulation shows the direct dependence between the scanning pitch and the curvature square root, when the curvature radius is maintained constant.

$$\sqrt{K} = \frac{p}{\rho} \tag{4}$$

where:

p = acquisition pitch; K= Gaussian curvature; ρ = sphere radius.

In a previous work [15] it has been assumed that Free-Form surfaces could be decomposed and approximated by a number of connected elementary geometries such as spheres, cylinders, cones etc. These assumptions could be referred to in order to move from the ideal sphere case which has been used as benchmark, to more generalised Free-Form geometries. In fact, evaluating a generic osculating geometry to the Free-Form surface, it is quite impossible to find small elementary radiuses ρ because of its smooth behaviour.

As shown in the formula (4), working with small pitches while acquiring simple geometries, that reasonably represent the ideal behaviour of Free-Form surface, it could lead to neglect this former curvature component. In fact, (4) shows that if the scanning pitch linearly tends to zero, the curvature *K* also do the same, with a faster behaviour.

2.1.2 Curvature *K* metrological noise and geometrical anomalies component formulation

Moving the attention on the latter component of the proposed Free-Form formulation, involving all the components that are not connected with the nominal smooth geometry described in the previous discussion, and which could be related with geometrical anomalies or with acquisition noise.

Focusing on all those curvature features which cannot directly be correlated to ideal geometry characteristics, a new set of experiments have been developed, thus generating some different benchmark geometries, which have been characterised by a nominal curvature profile in addition to a Gaussian statistical noise with noun average and different values of standard deviation.

Working with different values of variance for the statistical noise, the standard deviation of the measured curvature *K*, on the whole surface, has been evaluated. As the difference between the ideal curvature profile and the noise characteristics has to be demonstrated, two different surfaces have been analysed, in order to show the ideal curvature uninfluence, if compared to the noise effort. For these reasons, a simple plane with the addition of the Gaussian statistical noise *I* (Fig. 6) and another surface characterised by a known curvature profile (Fig. 7) with the addition of the same previous noise have been designed as benchmarks.

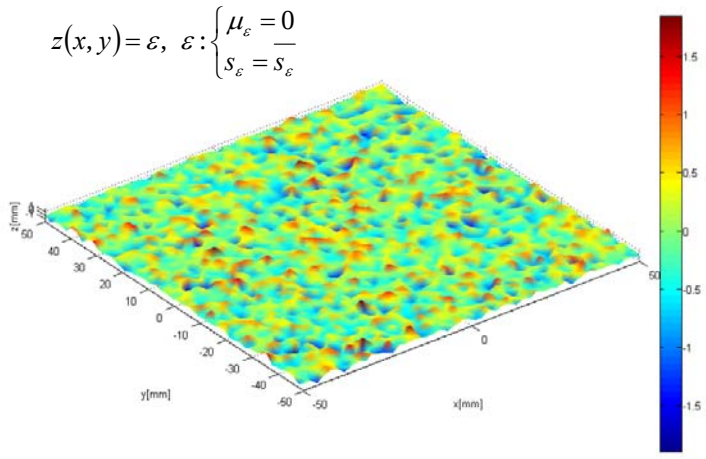

Figure 6: noised planar benchmarking surface.

The latter surface has been designed in order to show a significant curvature profile along all radial directions, with both harmonic and exponential behaviour. These expedients ensure a wide range of possible curvature combinations in any directions.

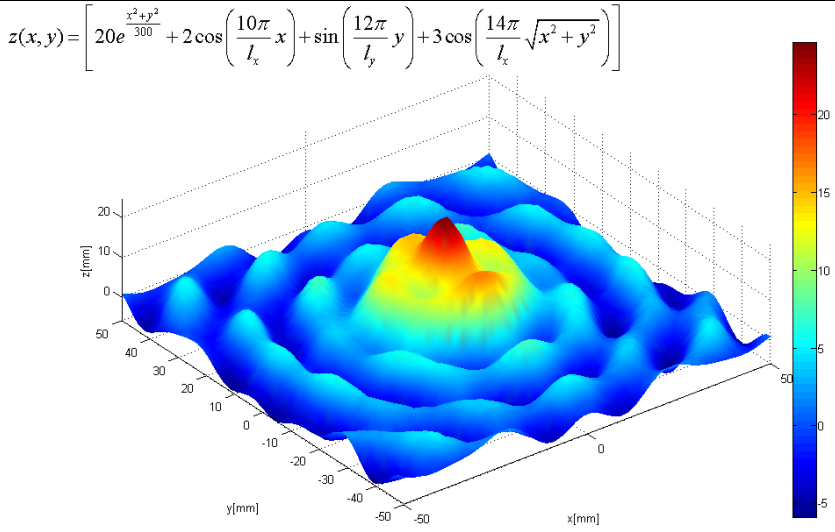

Figure 7: non-zero curvature benchmarking surface without noise.

This approach has been followed in order to find similarities between the behaviour of the Free-Form

surfaces affected by geometrical anomalies or acquisition noise and elementary geometries with the same characteristics: in fact, if the ideal curvature profiles of two different noised surfaces, the former very complicated and the latter much more simpler (such as a planar one), would result to be very similar, great benefits could be achieved in studying Free-Form curvature behaviours, because the anomalies distribution on a benchmarking plane could be taken as reference for any other cases.

Comparing the outputs obtained for the standard deviation (Tab. 2) (Fig. 8) of the Gaussian statistical noise and the standard deviation of the curvature *K* both for the plane and the second surface, the two behaviours appear without significant differences.

σ_I [mm]	σ_K [rad] (non-zero noised curvature profile)	σ_K [rad] (noised planar profile)
0,125	0,143	0,024
0,250	0,198	0,093
0,500	0,303	0,298
1,000	0,716	0,798
2,000	1,416	1,571
3,000	2,003	2,156
4,000	2,398	2,434
5,000	2,763	2,770
6,000	2,998	3,073
7,000	3,185	3,257

Table 2: experimental behaviour of StD for curvature vs Gaussian statistical noise on *z* coordinate

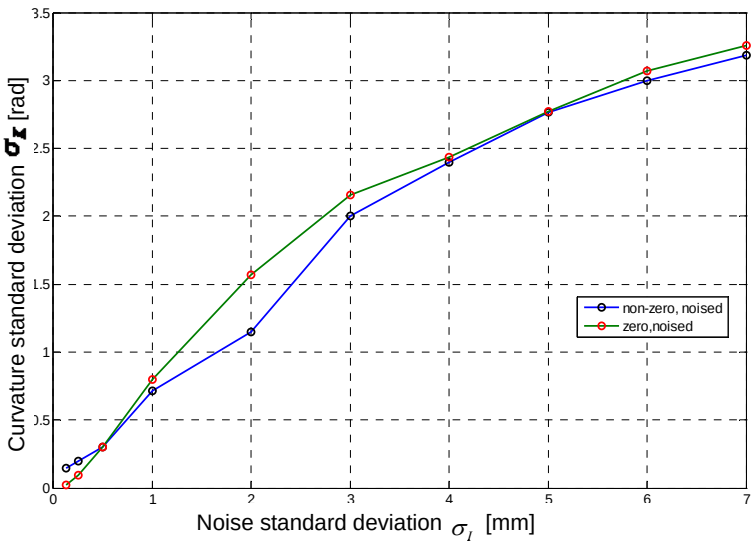

Figure 8: experimental behaviour of StD for curvature vs Gaussian statistical noise on z coordinate

In order to get a mean relation between curvature *K* standard deviation s_K and the known Gaussian noise standard deviation s_I, which has been just represented (Fig. 8), it has been necessary to identify a model

synthesising the non-nominal component of curvature *K*. A plane with a single perturbed point has been designed (Fig.9) because working on a planar set of points, if a Gaussian statistical perturbation were added to a single point, then it would have been possible to measure the curvature *K* on the perturbed point, thus identifying its correlation with the acquisition pitch.

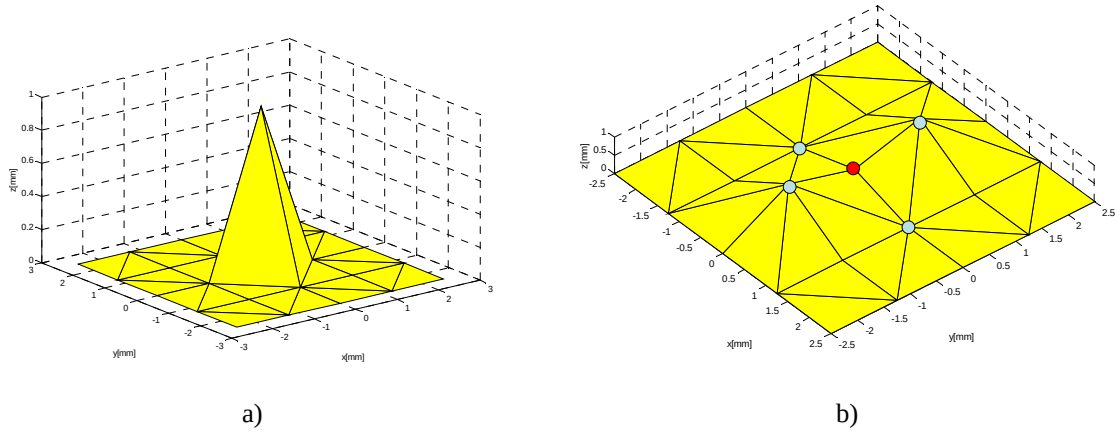

a) b)

Figure 9: plane with a single perturbed point a) positive curvature neighbourhood; b) negative (saddle) curvature neighbourhood

Before going beyond with model identification, it must be regarded that modelling strategies of positive and negative curvature *K* show significant differences [15].

The formulation of the positive curvature *K* will be then [15]:

$$K = 2\pi - 4\arccos\left(\frac{I^2}{p^2 + I^2}\right) \tag{5}$$

where *I* is measured perturbation intensity (Fig.9a) and *p* is the acquisition pitch.

On the other hand, I cannot be considered as a generalised parameter able to describe the non-nominal components of the curvature. In fact, it is related to the *z* coordinate.

This particular problem can be solved considering that Gaussian statistical noise has zero average. Furthermore, the upper and lower bounds of the *z* coordinate variation interval, due to the presence of the noise, can be obtained with a precise confidence level, if the hypothesis of normal distribution is assumed.

In the specific, assuming a confidence level equal to 68,27% means to adopt a unitary covering factor [18], because the unique noised point, which the model is based on, can be seen as a single sample of the entire population made up of all the noised points belonging to the original cloud.

The following expression gives the value of the *z* coordinate noise upper limit:

$$I = \mu_I + \sigma_I = \sigma_I \tag{6}$$

Considering the upper bound of the *z* coordinate variation interval to be the most significant one, in order to calculate relevant curvature values, thanks to Equation (6) and assuming the previously defined confidence level, the deviation parameter σ_I can be substituted to *I*.

It is now possible to derive the relation $p = p(K, I)$ by simply inverting equation (5) and introducing equation (6). This pitch formulation can be written also as $p = p(K, \sigma_I)$.

$$p = I\sqrt{\frac{1-\cos\left(\frac{2\pi - K}{4}\right)}{\cos\left(\frac{2\pi - K}{4}\right)}} = s(I)\sqrt{\frac{1-\sin\left(\frac{K}{4}\right)}{\sin\left(\frac{K}{4}\right)}} \tag{7}$$

Equation (7) shows the dependence of the scanning pitch *p* from the deviation parameter σ_I, but it must be regarded that the standard deviation of the *z* coordinate noise can't still be considered a valid generalized parameter in order to describe local surface complexity.

As curvature has been proved to be a powerful intrinsic morphological descriptor [15], it would be much more better using the curvature standard deviation σ_K, which has been graphically shown to be related to the parameter σ_I in Fig. 8, reflecting data reported in Table 2.

Considering that I follows a normal distribution which probability density equation is:

$$f(I) = \frac{1}{\sqrt{2\pi}\sigma_I} e^{\left(-\frac{I^2}{2\sigma_I{}^2}\right)} \tag{8}$$

The corresponding *K* probability density, when such a perturbation is applied to the *z* coordinate, can be obtained by the following formula [18]:

$$f(K) = \left|\frac{d}{dK} I(K)\right| f(I(K)), \tag{9}$$

where the function *I(K)* can be obtained from formula (5), ones defining a preliminary pitch value p_0. Remembering Equation (6), it follows that:

$$I(K) = \sigma_{I(K)} = p_0\sqrt{\frac{\sin\left(\frac{K}{4}\right)}{1-\sin\left(\frac{K}{4}\right)}} \tag{10}$$

The expression $\left|\frac{d}{dK} I(K)\right|$ can be also manually obtained by Equation (10) differentiation. Finally, the function

$f(I(K))$ can be easily obtained by substituting Equation (10) in Equation (8).

The K standard deviation σ_K is then obtained from the respective variance, calculated through the classical definition [18] applied to Eq. (9):

$$\sigma_K = \sqrt{\sigma_K^{\,2}} = \sqrt{\int_{-\infty}^{+\infty} f(K)\cdot\left(K-\mu_K\right)^2 dK} = \sqrt{\int_{-\infty}^{+\infty} f(K)\cdot K^2 dK} \qquad (11)$$

where μ_K is K statistical average evaluated on the whole surface: it has been experimentally demonstrated that this value tends to zero for Free-Form surfaces, because if those curvature values corresponding to the boundary zones are sufficiently small, all the negative curvature values measured on the internal points "compensate" the positive ones [17].

Thanks to these considerations, the definition proposed for the scanning pitch can be updated as follows:

$$p = p(K,\sigma_I) = p\left(K,\sigma_K\right), \qquad \text{K} > 0 \qquad (12)$$

As definition (12) shows, the optimal pitch formulation (7) depends on the curvature K, evaluated on the single point, but also on the curvature statistical distribution inferred for the whole surface, then using the standard deviation σ_K for the z coordinate standard deviation. The pitch behaviour for positive curvature values is also represented in the following figure.

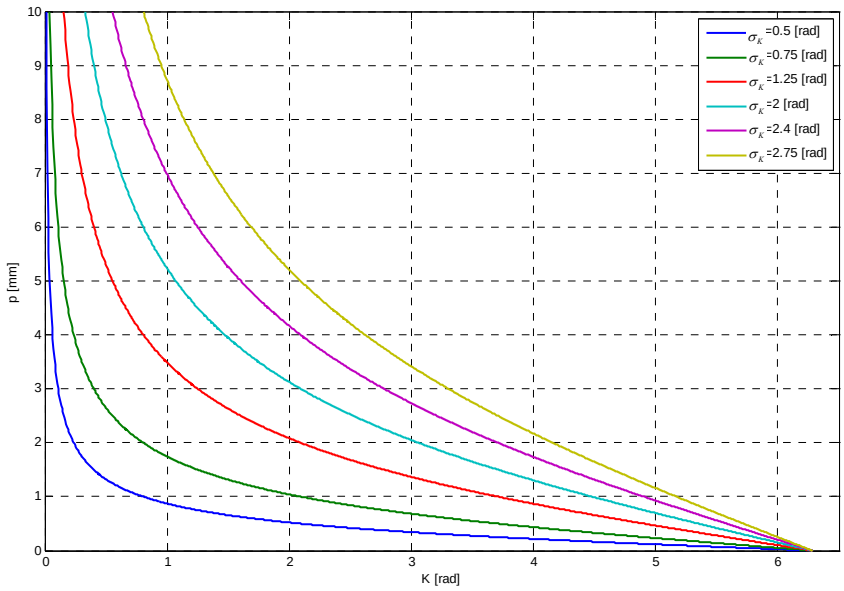

Figure 10: Pitch behaviour for positive curvature values for different values of s_k

When talking about the negative curvatures *K*, a method will be underwent similarly to what happened when deriving the pitch model for the positive curvature interval. As the typical saddle neighbourhood (Fig. 9b) is quite different from the positive curvature one, a different equation has been employed to formalize the pitch expression depending on the negative curvature *K* and the statistical characteristic σ_K.

Starting again from the definition of the nodal curvature *K* (1) as a function of a preliminary scanning pitch and the relative *z* coordinate (here called *I/2*) of single perturbed node, as previously defined for positive curvatures, Equation (7) have been modified in the following way:

$$K = 2\pi - 4\arccos\left(-\frac{I^2/4}{p^2 + I^2/4}\right) \tag{13}$$

The pitch formulation can be obtained again from Equation (13), by introducing the equivalence relation (6) and following few steps. Even dealing with negative curvature, the upper bound of the z coordinate variation interval can be considered to be the most significant one, in order to calculate relevant curvature values. Assuming a 68,27% confidence level, the deviation parameter σ_I can be again substituted to I.

$$p = \frac{\sigma_I}{2}\sqrt{-\frac{1+\cos\left(\frac{2\pi - K}{4}\right)}{\cos\left(\frac{2\pi - K}{4}\right)}} = \frac{\sigma_I}{2}\sqrt{-\frac{1+\sin\left(\frac{K}{4}\right)}{\sin\left(\frac{K}{4}\right)}} \tag{14}$$

Again it is possible to employ the relation between σ_I and σ_K obtainable from Table 2, in order to enter formula (14) for pitch definition when curvature *K* has negative values. The behaviour of the proposed pitch function in the negative curvatures interval is quite similar to the graph related to Equation (7) and can be obtained as a mirror of that represented in Fig. 10.

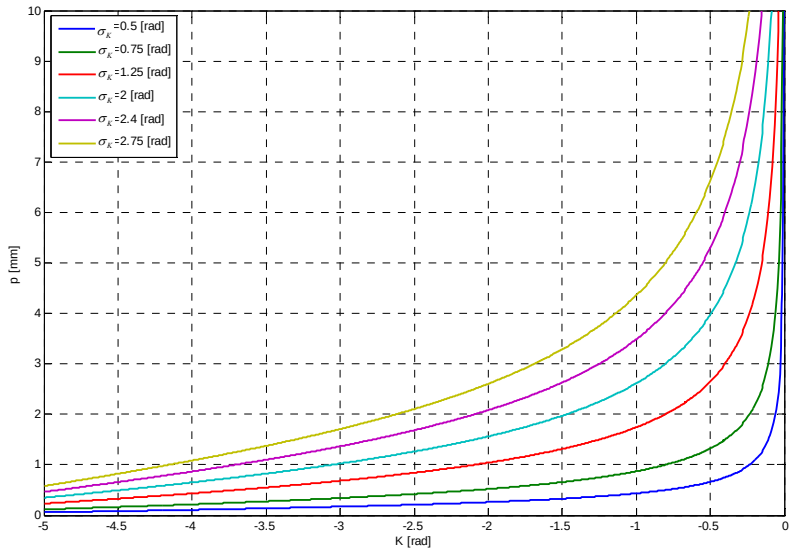

Figure 11: Pitch behaviour for negative curvature values for different values of σ_K

Considering previous assumption about a former component of the curvature K, which is related to purely geometrical features characterising Free-Form surfaces and tends to zero with the pitch reduction, it is possible to identify the adaptive pitch function using Equation (14) for $K < 0$ and definition (7) for $K \geq 0$. Each branch depends on the parameter σ_K (Fig. 12)

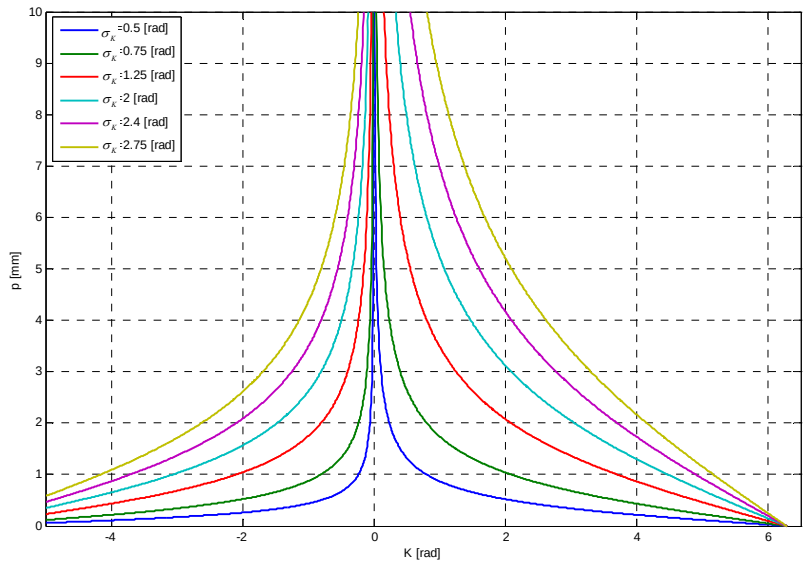

Figure 12: Pitch behaviour for positive and negative curvature values for different values of s_k

Even if the pitch functions represented in Fig. 12 show asymptotic behaviour when getting close to small curvature values, the largest grid dimension available on a specific 3D Scanner could act as a upper limit for the pitch existence interval (as instance, the Roland Picza PIX-30 scanning device works on a grid dimension range from 0,05mm to 10mm) [19].

2.2 Points cloud management strategy

A new pitch could be proposed for every points of the cloud, thanks to the function just described (Fig. 12), in order to design a new efficient sampling plan depending on the local curvature map. Working on Formula (7) and (14), the sampling plan is codified with a new pitch map which is correlated to the curvature one on every node. Two different approaches have proved to be necessary in order to manage de-fitting and in-fitting operations. In the former case (Fig.13), the preliminary grid has been modified basing on *raster* logic concepts [20]:

- all the preliminary points with the same new pitch proposed, have been aggregated in classes;
- once considered one single class, the points cloud has then been split in sub-domains, thanks to the use of a grid characterised by a modular dimension equal to the new proposed pitch;
- working on every sub-domains which middle point can be evaluated, all the points associated to the proposed pitch has been erased, except for the nearest point to the middle one.

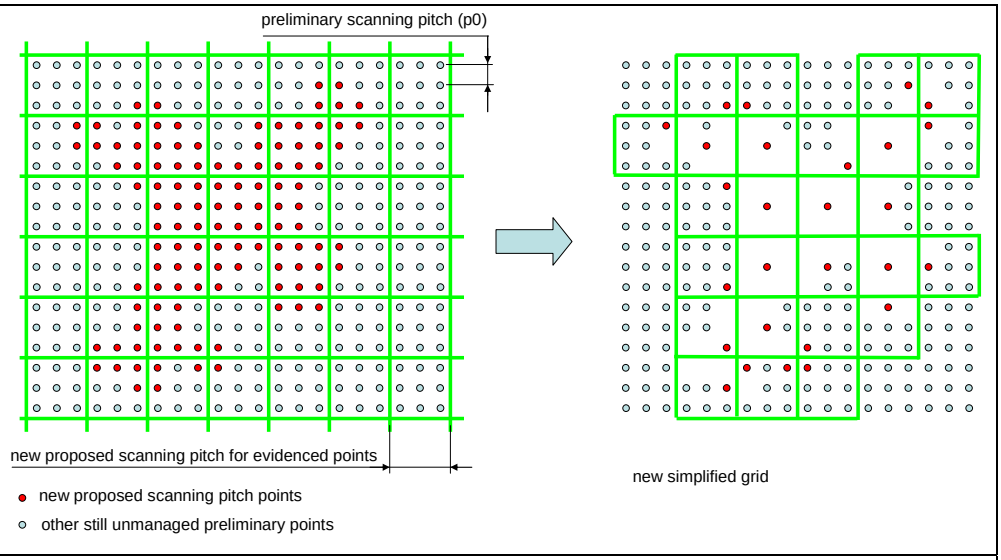

Figure 13: De-fitting points cloud management strategy

When dealing with in-fitting management, a *raster*-logic strategy for grid modification could still be employed with the following steps:

- the previous class subdivision is maintained. Only one class is considered, which proposed pitch is smaller than the preliminary one;
- once considered one single class, a grid is still employed, characterised by a modular dimension equal to the preliminary pitch, in order to split the cloud in sub-domains;
- working on every sub-domains, a new grid characterized by the proposed pitch as specific dimension, has been designed (Fig.14).

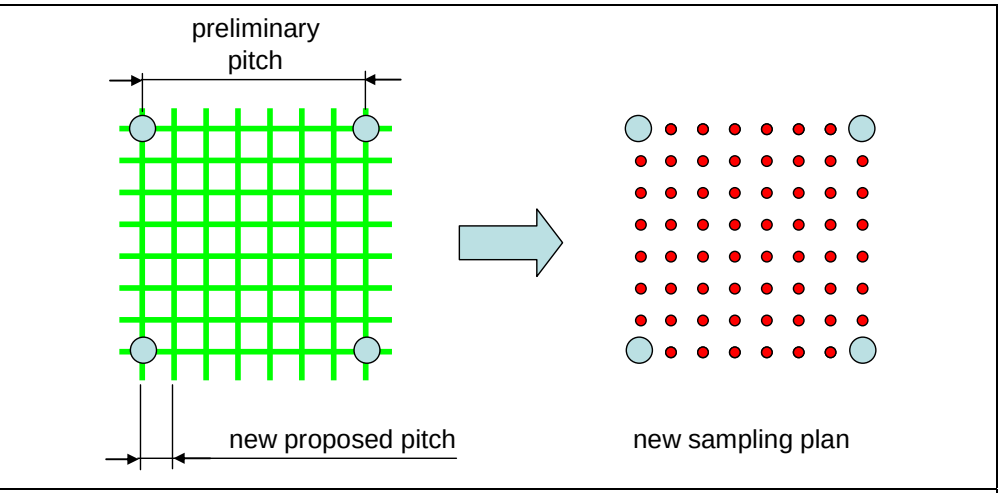

Figure 14: in-fitting points cloud management strategy

At this stage, a new sampling plan is ready to be implemented on the 3D scanner.

3.0 Experimental Validation

In order to verify the effectiveness of the proposed approach, that aims to provide to the following reverse engineering cycle phases a well organised points cloud for a virtual mathematical model reconstruction, it has been decided at first to compare it with a standardised methodology, that at the same of the present approach connects points clouds with virtual models analysing the local morphological complexity and then to implement some case studies.

For the first test, the specimen employed has been the STL files generation methodology, that even if it works with an opposite direction *(virtual mathematical model -> 3D mesh)*, if compared with the Reverse Engineering Cycle *(3D mesh -> virtual mathematical model)*, it is recognised as a standard in the codification between virtual mathematical models and mesh ones and, at the same of the proposed approach, is based on Discrete Curvature evaluation and Optimal Pitch calculation [16]. Approximating a continuous, differentiable surface, the approximating triangles dimension in fact, usually goes with the local morphological surface complexity. In other words, STL conversion gives a non-redundant set of approximating points (i.e. a "point cloud") characterized by variable points density (Total Deviation Filter) (Fig. 15).

So starting from the previous equations (14) it is possible to compare from a numerical and graphical point of view the behaviour of the two functions (STL and proposed methodology) correlating the proposed pitch p and the curvature K both by the STL generation both by the proposed methodology.

Looking at the results of the graphical and numerical comparison (Fig. 8a), it is possible to see that the two curves show a similar behaviour providing also some overlapping zones. This underlines that the proposed method is able to provide an interesting reliability and resolution level comparable with that one obtained by the STL method implementation.

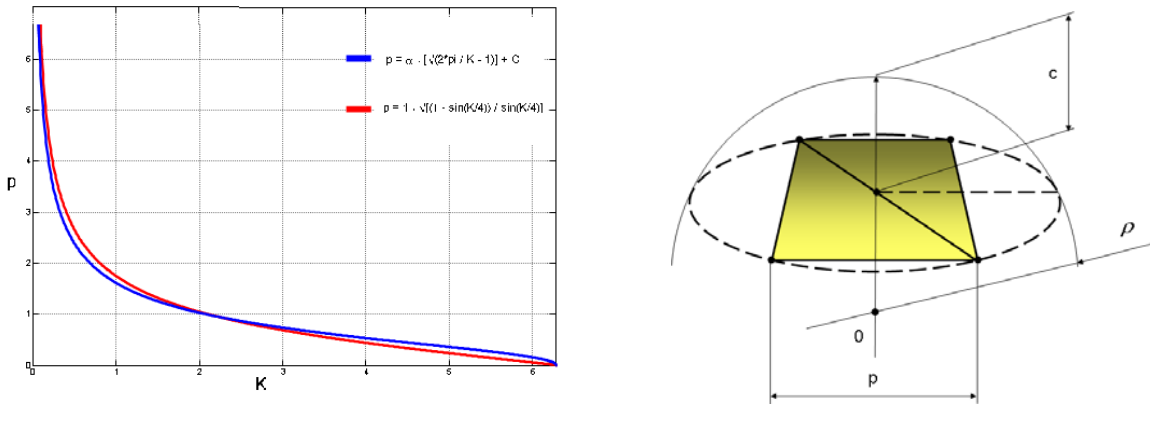

Figure 15: "Total Deviation Filter"; a) comparison between the pitch Function obtained through the application of a "Total Deviation" threshold (blue), and that represented also by Eq.14, derived from local Curvature Analysis; b) "Total Deviation" Approach; c represents the Deviation amount, between the original Surface (white) and the approximating triangulation (yellow)

In order to verify also the behaviour of the approach proposed with the use of some case studies and working directly on a 3D scanner, two free-form geometries has been selected as benchmarks. Working with a Roland Picza 3.0 3D scanner the benchmarking geometries (Fig.16,20) has been acquired working two different preliminary pitches, one very sparse and one very crowd, in order to have a more consistent data set about the

proposed methodology behaviour.

Figure 16: First benchmarking geometry employed for the proposed method validation

Both the two benchmarking geometries selection could be justified by the necessity to employ an object characterised by significant differences in term of morphological complexity and in particular of curvature *K* (Fig.16,20). While the more flat regions could be acquired with a very spare point cloud, because their complexity level is quite low, the other zones, that show higher complexity levels should be described with a more detailed acquisition pitch in the composition of the sampling plan that the method will provide.

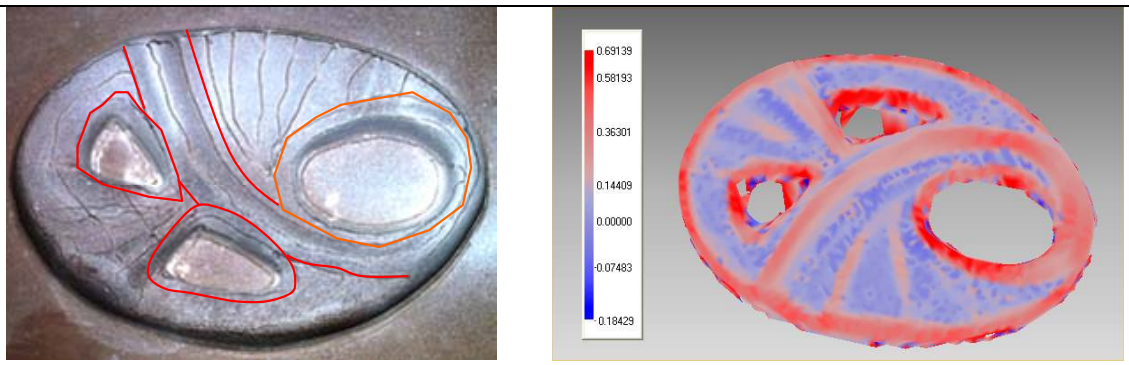

a) b)

Figure 17: First benchmarking geometry employed for the proposed method validation with a) evidenced most morphological significant zones (red lines) b) curvature map

Working with a 3D scanner which highest acquisition pitch is 10 mm it is possible to hypnotize that the more planar zones, corresponding to those zones represented with blue colour (Fig.17b, 21b), should be codified as regions that needs the highest pitch possible, sparse points cloud, while the others characterised by red colour (Fig.17b,21b) will ask a more detailed pitch. The sampling plan should be completed also by the presence of some regions in which the pitch will be a compromise between the largest and the most detailed ones.

So in order to verify the proposed methodology behaviour working on the first benchmark (Fig.16) the preliminary acquisition has been set to 5mm, half of the biggest pitch that Roland Picza 3D scanner is able to provide, both along the x and y acquisition axes for the first benchmark, in order to verify the methodology

behaviour starting from a sparse points clouds.

Working directly on the obtained point cloud (Fig.18,22) the algorithm implementation has suggested a new sampling plan employing a colour code (Fig.19,23).

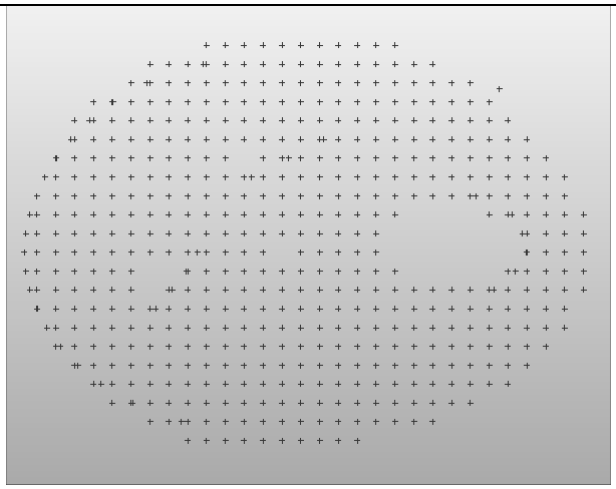

Figure 18: First benchmarking geometry preliminary points cloud

The results obtained on the first benchmark (Fig. 19) by the algorithm implementation show that the zones close to the holes and the main central rib should be reduced (dark violet), proposing a pitch close to 1 mm, while the already explained flat regions would need the widest pitch possible, around 10 mm, (light yellow).

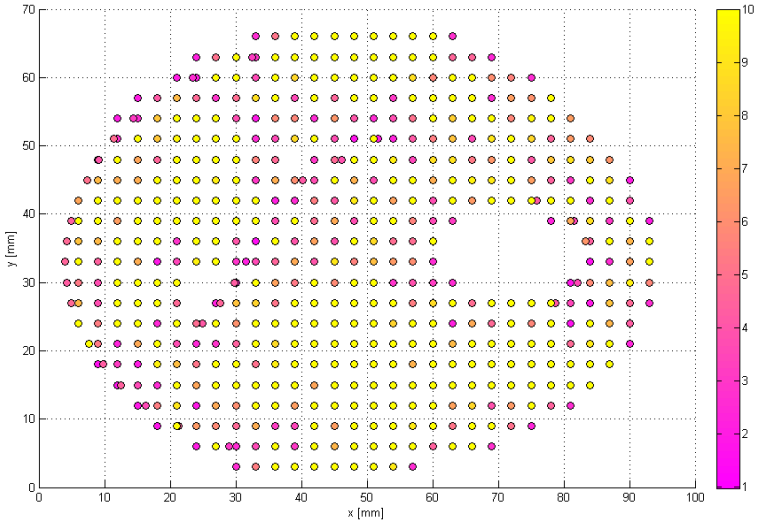

Figure 19: Suggested selective sampling plan (the colour bar values are the suggested pitches [mm])

Only few zones show that the preliminary pitch, 5 mm, (orange) could be the right solution inside the efficient sampling plan.

For the second benchmark the preliminary acquisition pitch has been fixed to a more detailed value, 1 mm, in order to verify also the algorithm behaviour starting from a more crowd points cloud.

Figure 20: Benchmarking geometry employed for the proposed method validation

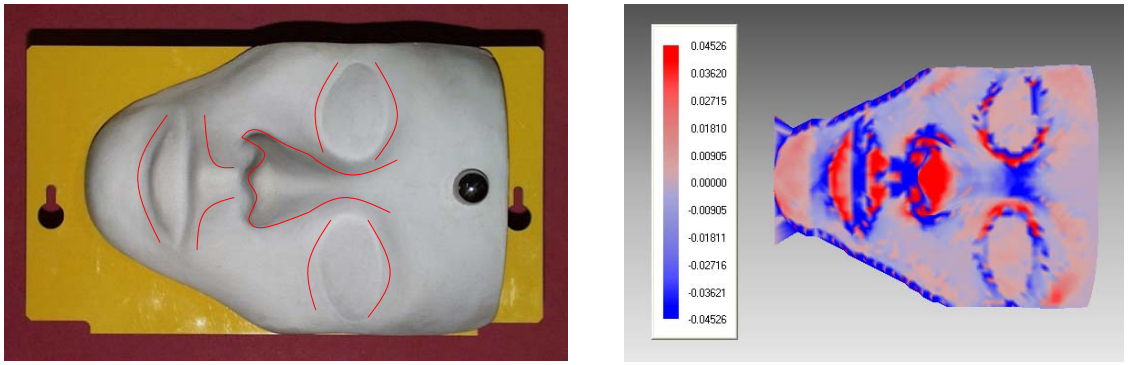

a) b)

Figure 21: Benchmarking geometry employed for the proposed method validation with a) evidenced most morphological significant zones (red lines) b) curvature map

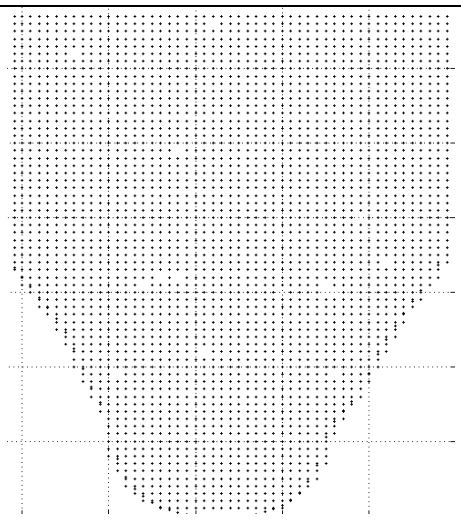

Figure 22: Suggested selective sampling plan (the colour bar values are the suggested pitches [mm])

The results obtained on the second benchmark (Fig.20) by the algorithm implementation show that the

zones close to the eyes, the nose and the lips should be maintained to the actual pitch (dark violet), proposing a pitch close to 1 mm, while the other zones, with a more stable and flatness morphological behaviour, would need an higher pitch, around 8mm, (dark yellow). Only few zones show an intermediate pitch (orange) as efficient solution for the sampling plan of this geometry.

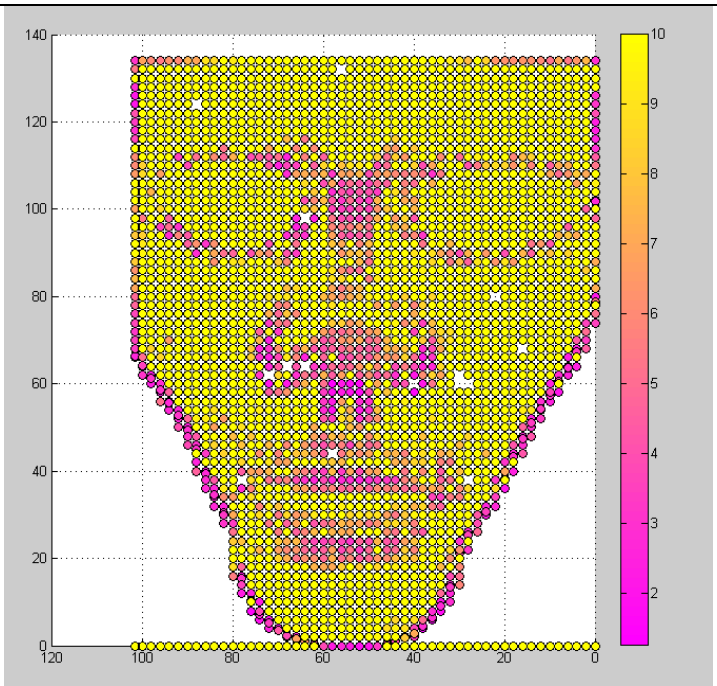

Figure 23: Suggested selective sampling plan (the colour bar values are the suggested pitches [mm])

In order to verify the reliability of the proposed sampling plan, it has been implemented in order to obtain the suggested points clouds and to verify it again trough the proposed algorithm.

As it is possible to see in the next figure (Fig.24,25) the new analysis developed on the results of the suggested sampling plan confirms that the new series of proposed pitches are able to provide a set of morphological data that are enough to describe in reliable way the morphological behaviour of the two surfaces acquired.

4.0 Conclusion

Even if the methodology has been experimented working with a contact 3D scanner, that anyway is very significant considering all the possible applications where it could be employed and the very low cost, this approach could be employed also working with other systems. When in fact it is necessary to have precise information about the morphology of an object, for example a mechanical component, often the 3D non contact scanners (laser scanner, laser radar, …) are not so reliable. So in this situation the best choice could be the use of a CMM machine. But working with a CMM it is impossible to employ a constant grid during the acquisition because it would employ too much time in order to acquire the entire object. For this reason the solution could be the integration of more than one 3D scanner, for example the 3D laser scanner for the preliminary acquisition and then a CMM machine or the Roland Picza for the deeper one, but working with an optimised selective sampling plan.

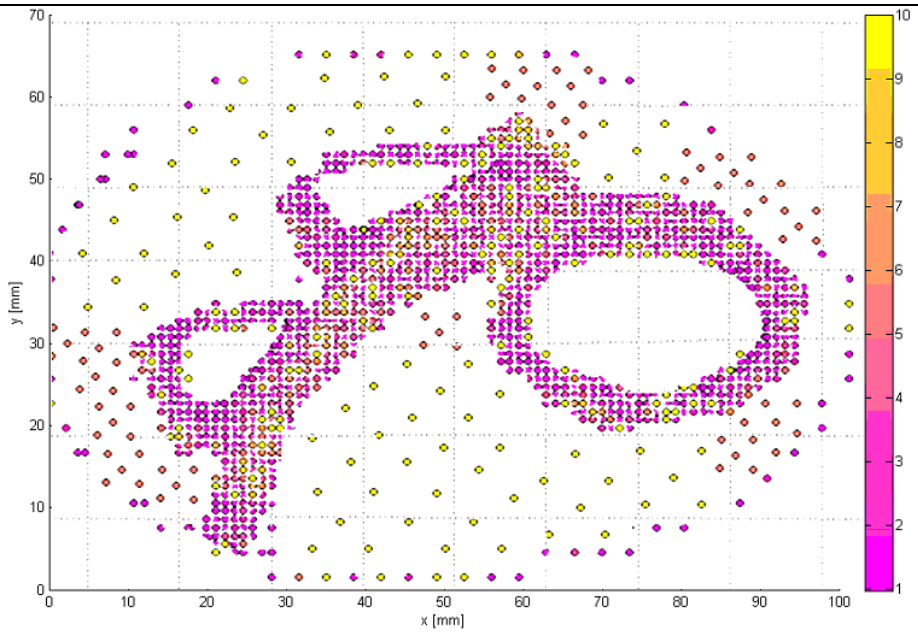

Figure 24: example of points cloud employed for the methodology validation and obtained working on a human face calc

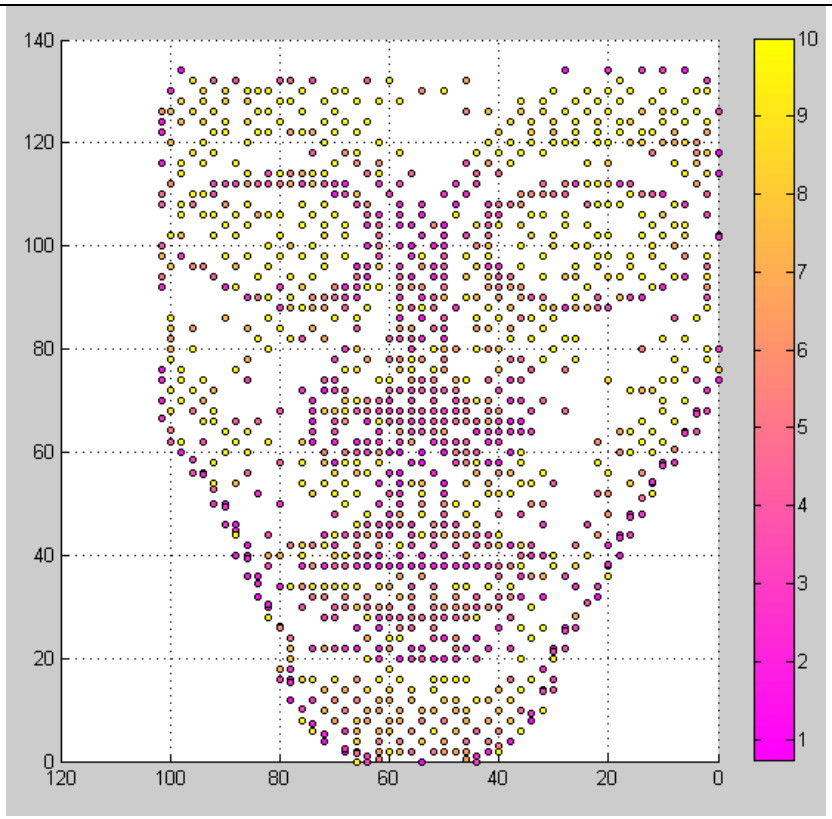

Figure 25: example of points cloud employed for the methodology validation and obtained working on a human face calc

For this reason the possibility to have a methodology that provides an efficient sampling plan for Free-Forms acquisition is very important. The solution proposed provides in fact a strategy selecting the most efficient

pitch dimensions working with the local complexity of the geometry acquired and the metrological performances of the 3D scanner employed. If in fact the 3D scanner provides a very noisy points cloud the methodology will suggest a quite flat pitch selection introducing already also for little curvature values a little pitch that will be reduced of small percentages proportionally with the curvature *K* increasing, considering the verified behaviour that decreasing the pitch dimension when the points cloud shape is mainly characterised by anomalies the curvature values does not decrease. Working with less noisy points clouds the methodology will be more able to employ selective pitches for every curvature values identified. In this scenario if in fact the methodology suggests decreasing the pitch dimension the curvature value *K* obtainable will decrease, so it will not be necessary to develop a successive deeper acquisition in that zone because the present morphological information will be enough.

References

1. Varady T, Martin RR, Cox J. (1997), "Reverse engineering of geometric models—an introduction", Computer-Aided-Design 1997, 29(4), pp. 255–268
2. Bidanda B, Harding K., (1991) "Reverse Engineering: an Evaluation of prospective non contact technologies and applications in manufacturing systems", Int. J. Computer Integrated Manufacturing, Vol 30, No 10, pp.791 – 805.
3. Chua C K, Chou S M, Ng W S, Chow K Y, Lee S T, Aung S C and Seah C S, (1998) "Integrated Experimental Approach to Link Laser Digitizer, CAD/CAM System and Rapid Prototyping System for Biomedical Applications, International Journal of Advanced Manufacturing Technology, Vol 14, pp 110-115.
4. Cheah C.M., Chua C.K., Tan K.H. and Teo C.K., (2003) "Integration of Laser Surface Digitising with Computer-Aided Design and Manufacturing for Developing Facial Prostheses - Part 1: Design and Fabrication of Prostheses Replicas, International Journal of Prosthodontics, Vol 16, Number 4, pp 435-441, Jul - Aug 2003.
5. Cheah C.M., Chua C.K., Tan K.H. and Teo C.K. (2003) Integration of Laser Surface Digitising with Computer-Aided Design and Manufacturing for Developing Facial Prostheses - Part 2: Development of Moulding Techniques for Casting Prosthetic Parts, International Journal of Prosthodontics, Vol 16, Number 5, pp 541-546, 2003.
6. Sarfraz M., (2006), "Computer-aided reverse engineering using simulated evolution on NURBS", Virtual and Physical Prototyping; December 2006; Volume 1 No. 4 Pages 243 - 257
7. Creehan K.D., Bidanda B., (2006), "Computer-aided reverse engineering of the human musculoskeletal system, Virtual and Physical Prototyping; June 2006; Volume 1 No. 2 Pages 83 - 91

8. Amenta, N., Bern, M., (1999), “Surface reconstruction by Voronoi filtering”, Discrete Comput. Geom. Vol. 22 (4), pp. 481–504.
9. Ciarlet, P.G., Raviart, P.-A., (1972), “General Lagrange and Hermit Interpolation in Rn with applications to the finite element method”. Arch. Rational Mesh. Engrg. Vol 46, pp. 177–199.
10. Sarkar B, Menq C-H., “Smooth-surface approximation and reverse engineering”, Computer-Aided Design 1991; Vol 23(9) pp. 623–628
11. Weekenmann A, Eitzert H, Garmer M.,Weber H., (1995), “Functionality oriented evaluation and sampling strategy in coordinate metrology”, Precision Engineering 1995, Vol. 17, pp. 244-252
12. K. Kase, A. Makinouchi, T. Nakagawa, H Suzuki, F. Kimura, “Shape error evaluation method of Free-Form surfaces”, Computer Aided Design 1999, Vol. 31, pp. 495-505
13. Cho M, Kim K., (1995). “New inspection planning strategy for sculptured surfaces using coordinate measuring machine. International Journal of Production Research 1995; Vol.33: pp.427–444.
14. Li X., Barhak J., Guskov I., Blake G. W., (2007) “Automatic registration for inspection of complex shapes”, Virtual and Physical Prototyping; 2007, Vol.2 (2), pp. 75 – 88
15. A. Courtial, E. Vezzetti, (2008),” New 3D segmentation approach for reverse engineering selective sampling acquisition”, International Journal of Advanced Manufacturing Technology, Vol. 35, pp. 900-907
16. Mortenson M. 1989, “Geometrical Models in Computer Graphics”, McGraw-Hill Editor
17. Greco S., Valabrega P., (1992), “Lezioni di algebra lineare e geometria”, Levrotto e Bella Editor
18. Vicario G., Levi R., (1998), “Calcolo delle probabilità e statistica per ingegneri”, Progetto Leonardo Editor
19. Iuliano L., Vezzetti E., (2000), “Application of a piezoelectric reverse engineering system to the jewellery prototyping”, CIRP – ICME Conference Proceedings, Capri, pp.253 - 263.
20. Hoffman R, Jain AK., (1987),”Segmentation and classification of range images”, IEEE Transactions on Pattern Analysis and Machine Intelligence 1987;Vol. 5, pp. 608–620.